ELSEVIER

Marine Chemistry 72 (2000) 151–169

MARINE CHEMISTRY

www.elsevier.nl/locate/marchem

The role of the annual cycles for the air–sea exchange of CO_2

Göran Broström *

Department of Earth, Atmospheric and Planetary Physics, Room 54-1424, Massachusetts Institute of Technology, 77 Massachusetts Avenue, Cambridge, MA 02139 USA

Received 31 May 1999; received in revised form 2 December 1999; accepted 8 August 2000

Abstract

The annually integrated air–sea flux of CO_2 is governed by two quantities: the basic state of the ocean (e.g., the properties of the winter mixed layer) and the signal from the annual cycles. In this study, I focus on the role of the annual cycles in mixing, sea-surface temperature and biological production. By integrating these cycles, it is shown that the annually integrated flux of CO_2 can be written as $F = \alpha(C_T^W - C_{Eq})$, where F is the mean annual air–sea flux of CO_2, α is an equilibrium rate constant (m/year), C_T^W is the total dissolved inorganic carbon concentration in the winter mixed layers and C_{Eq} is the dynamic equilibrium concentration for C_T^W. In the formula, α and C_{Eq} capture the influence of the annual cycles as well as the spatial variations in, for example, the alkalinity. I analyze data from the Ocean Weather Stations (OWS) in the North Atlantic and some results from the MIT biogeochemical ocean model to find adequate descriptions of α and C_{Eq}. According to these model/data estimates, the influence of the annual cycles in sea-surface temperature and biological production on the dynamic equilibrium concentration is on the order of -5 to -20 and 0–30 μmol/kg, respectively. These numbers are not negligible showing that the annual cycles must be considered when analyzing the oceanic carbon cycle. The spatial distribution of the quantities C_T^W, α, and C_{Eq} are estimated for the North Atlantic using data from the TTO/NAS expedition and a combination of model and data analyses. The air–sea flux is calculated according to the above formula, and the seawards flux is estimated to be 0.4 Gt C/year for the area north of 30°N.

Keywords: Carbon cycle; Air–sea flux; Modeling; Annual cycle; Mixing

1. Introduction

The present release of CO_2 to the atmosphere is on the order of 6 Gt C/year (Marland et al., 1998). Of the anthropogenic released CO_2, about 50% goes to an increase in the atmospheric partial pressure of CO_2. The remaining CO_2 is either taken up by the land-based biomass or is dissolved in the ocean (Broecker and Peng, 1982). However, the division of the total sink of anthropogenic CO_2 into the terrestrial and oceanic sinks is still uncertain (Keeling et al., 1996; Fan et al., 1998; Lee et al., 1998; Stevens et al., 1998). For predictions on future levels of CO_2 in the atmosphere, it is important to describe these sinks of the anthropogenic CO_2 in an adequate way. An intermediate step in this process is to understand the CO_2 fluxes in the natural system.

* Department of Oceanography, Earth Science Centre, Göteborg University, Box 460, S-405 30, Gothenburg, Sweden.

E-mail address: gobr@oce.gu.se (G. Broström).

0304-4203/00/$ - see front matter
PII: S0304-4203(00)00079-7

In this work, I focus on the air–sea flux of CO_2 in the mid to high latitudes of the North Atlantic, although the derived formalism may be applied at other locations. Following Liss and Merlivat (1986), the air–sea exchange of CO_2 may be written as:

$$F_I(t) = k(t)\,\alpha_{CO_2}(t)\left(pCO_2^{SW}(t) - pCO_2^{A}(t)\right). \quad (1)$$

F_I is the flux at time t; $\alpha_{CO_2}(t)$ is the CO_2 solubility in seawater (Weiss, 1974); pCO_2^{SW} is the partial pressure of CO_2 in seawater; pCO_2^{A} is the partial pressure of CO_2 in the atmosphere; and $k(t)$ is the gas exchange coefficient. Wanninkhof (1992) proposed that:

$$k = 0.31\left(\frac{660}{Sc}\right)^{1/2} W_{10}^2, \quad (2)$$

where k is given in cm/h, Sc is the Schmidt number (the ratio of molecular viscosity to molecular diffusivity for a substance), and W_{10} is the wind speed at 10 m height.

The air–sea flux of CO_2 is, thus, driven by the magnitude of the disequilibrium of the CO_2 pressure between the ocean and the atmosphere, and the exchange rate is given by the wind speed and the temperature of the sea surface (α_{CO_2} and Sc both depend on the temperature). In order to calculate the air–sea flux, it is necessary to analyze the strength and variability of the components in Eqs. (1) and (2). Notably, $k(t)\alpha_{CO_2}(t)$ depends mainly on the wind speed and can, thus, be evaluated from atmospheric data. The atmospheric pCO_2 has an annual amplitude of about 10 ppm (Conway et al., 1994); furthermore, the spatial variability is weak and the signal in pCO_2^{A} can be estimated from the global network of observation stations (Keeling and Whorf, 1996). However, its oceanic counterpart, pCO_2^{SW}, depends on the sea-surface temperature, the salinity, the total dissolved inorganic carbon concentration, C_T, and the total alkalinity concentration, A_T (Peng et al., 1987). The description of the air–sea flux of CO_2, therefore, requires knowledge of a number of highly coupled variables, such as the annual temperature cycles, wind speed, upwelling, and the biological production in the ocean (Takahashi et al., 1985b, 1993; Peng et al., 1987; Taylor et al., 1992; Follows et al., 1996; Stevens et al., 1998).

However, the large-scale features of the ocean change slowly as compared to the time scale of the annual cycle. Accordingly, it is reasonable to consider a separation of scales such that the annual cycles may be treated separately from the dynamics regulating the ocean-scale structure. Let us consider a situation where the properties of the winter mixed layer preconditions the structure of the coming annual cycle and thereby the air–sea flux of CO_2. The annually integrated flux of CO_2, F, is accordingly a function of the state of the winter mixed layer. Schematically, the flux may be written $F = F(C_T^W)$, where C_T^W is the total dissolved inorganic carbon concentration in the winter mixed layer. In a simplified manner, the annual air–sea exchange of CO_2 may be expressed as:

$$F = \alpha\left(C_T^W - C_{Eq}\right). \quad (3)$$

The above expression may be viewed as a linearized formula for the annually integrated air–sea exchange (Broström, 1997a,b).

In Eq. (1), α is an equilibrium rate constant (m/year), and C_{Eq} is the dynamic equilibrium concentration for C_T^W. C_{Eq} is defined as the wintertime total inorganic carbon concentration that would give zero annual flux of CO_2. Its definition does not represent a true equilibrium state, rather, it reflects a state that is always in disequilibrium, but where the net air–sea flux of CO_2 over the annual cycle is zero. The dynamic equilibrium concentration reflects the annual average of several processes and may be written as follows:

$$C_{Eq} = C_{Eq}^0 + \Delta C_{Eq}^{SST} + \Delta C_{Eq}^{Biol}. \quad (4)$$

Here, C_{Eq}^0 is the basic equilibrium state of the ocean: it is essentially defined as the C_T concentration that would make the winter mixed layer to be in equilibrium with the atmospheric pCO_2. ΔC_{Eq}^{SST} and ΔC_{Eq}^{Biol} reflect the influence of the SST and biological production cycles on the dynamic equilibrium concentration, respectively.

One of the advantages with a separation of the processes that controls the dynamic equilibrium concentration is that different data sources may be used to estimate the strength of each process. Further, results from different models may be intercompared in an adequate way, and various model results may

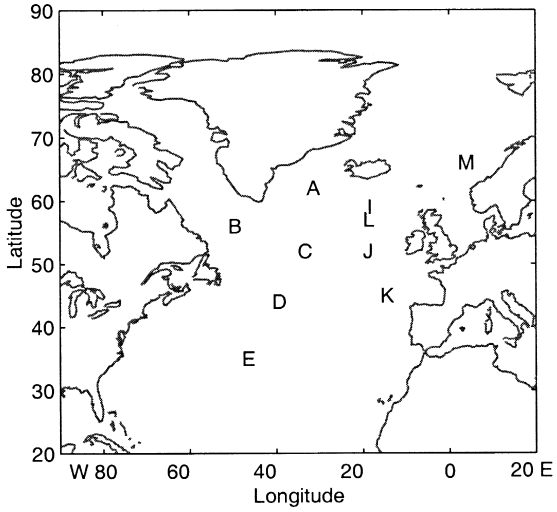

Fig. 1. The position of the different OWS used in this study. More details on the OWS are given in Table 1.

be used to find a relevant description of the processes that contributes to the dynamic equilibrium concentration. The quantities C_T^W and C_{Eq}^0 are defined from the state of the winter mixed layer and may be found directly from a data set (e.g., data from the TTO/NAS expedition; Brewer et al., 1986). The parameters α, ΔC_{Eq}^{SST}, and ΔC_{Eq}^{Biol} are tightly linked to the annual cycles and require detailed observations on the annual cycles to be evaluated. However, if it is possible to find a general description of α, ΔC_{Eq}^{SST}, and ΔC_{Eq}^{Biol}, the air–sea flux of CO_2 may be estimated in a consistent way from data taken at a single cruise.

In this study, I intend to investigate how α, ΔC_{Eq}^{SST}, and ΔC_{Eq}^{Biol} relate to the strength of the annual cycles by using a combination of data analysis and model results. Data required for this investigation are the following: the gas exchange coefficient (wind speed); the annual cycles in sea-surface temperature and biological production; and the vertical mixing cycle in the upper ocean. Some of these data are available from the network of Ocean Weather Stations (OWS), whereas others have to be estimated. The positions of the OWS stations are shown in Fig. 1 and some additional information on the stations can be found in Table 1. To describe the vertical mixing at the OWS, I use a one-dimensional model where the turbulent exchange coefficient is described by the k–ε scheme (Rodi, 1980, 1987). Some experiments with the MIT biogeochemical ocean model (Follows et al., 1996) are also analyzed and compared with the results of the one-dimensional model. The results from the modeling exercise are then combined with some estimates on the winter state, obtained from the TTO/NAS expedition data (Brewer et al., 1986), to find the air–sea flux of CO_2 in the North Atlantic.

Some model experiments are necessary to find the dynamics of each component in the system; these experiments are described in Section 2. The derivation and evaluation of α and C_{Eq} from these experiments are described in Section 3. In Section 4, data

Table 1
Some facts about the North Atlantic ocean weather ships used in this study

OWS	Position	Surf. obs.	T_r	$\langle 1 \rangle$	$\langle 1 + f(t) \rangle / \langle 1 \rangle$	a_{C_T}	α	ΔC_{Eq}^{SST}	$\Delta C_{Eq}^{Biol} / NO_3^W$
A	33°W, 62°N	1945–1973	7.3	105	0.55	2.0	114	−8.4	2.7
B	51°W, 56°N	1946–1974	5.5	112	0.55	2.1	129	−7.6	2.2
C	35°W, 52°N	1945–1982	8.7	114	0.52	1.9	115	−11.0	2.4
D	41°W, 44°N	1945–1973	16.9	106	0.59	1.7	106	−14.0	2.7
E	48°W, 35°N	1949–1973	21.7	65	0.50	1.6	53	−21.0	3.0
I	19°W, 59°N	1950–1975	10.4	106	0.61	1.9	121	−9.6	2.7
J	20°W, 52°N	1950–1975	12.1	103	0.62	1.8	116	−10.4	2.5
K	16°W, 45°N	1949–1975	15.0	81	0.62	1.7	88	−13.0	2.4
L	20°W, 57°N	1975–1982	10.9	119	0.60	1.9	132	−5.3	2.7
M	2°E, 66°N	1949–1992	8.3	92	0.62	1.8	110	−10.1	3.0

See text for details on the parameters that are shown.

from the TTO/NAS expedition are used to interpret the properties of the winter mixed layer and to calculate the air–sea flux of CO_2 in the North Atlantic. Finally, the results of this study are discussed in Section 5.

2. Some experiments on the annual cycles

It is useful to consider the basic features of the system before outlining the strategy for the experiments considered in this section. If the winter water is not in equilibrium with the atmosphere, there will be a gas exchange with the atmosphere. The response of the ocean depends on the mixing cycle (this process is investigated in Section 2.1). The sea-surface temperature and the biological production cycles influence pCO_2^{SW} and the effect of these annual cycles must be identified (see Sections 2.2 and 2.3, respectively). Finally, advection is also an important process, and it is discussed in Section 2.4. An important assumption in this study is that the system can be described in linear terms and that the strength of each process can be determined by a single experiment.

The depth over which the CO_2 from the air–sea exchange is distributed is an important factor in this study (i.e., the depth that is directly influenced by the air–sea gas exchange). The strength of the upper ocean mixing is estimated by using a one-dimensional mixing model that is based on the k–ε scheme (Rodi, 1980, 1987) (see Appendix A). The total dissolved inorganic carbon concentration is included in the model, and the air–sea flux is calculated according to Eqs. (1) and (2). In all experiments, the integration starts on March 1 and the model is integrated for 1 year. These experiments are carried out for each OWS, but I will mainly present results from station C.

An estimate of the mixed layer depth at station C is displayed in Fig. 2. The experiment shows that there is a strong interannual variability in the characteristic mixing depth. Nevertheless, there is generally an intermittent deep reaching mixing during the winter months. Any signals from the summer months are, therefore, reset each winter. In April, the mixing depth decreases, and the upper ocean is characterized

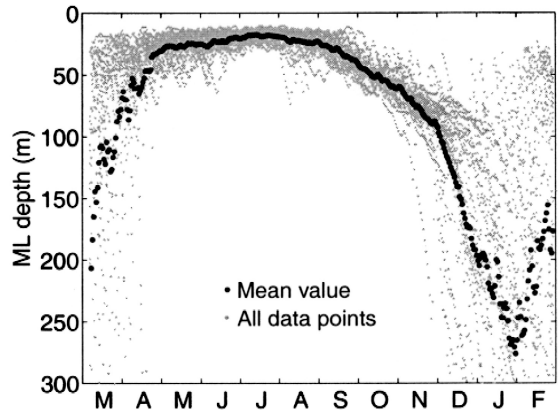

Fig. 2. An estimate of the mixed layer depth at OWS C. The gray dots represent model results from all of the years when there is forcing available, and the black dots represent the daily mean of these model runs. The mixed layer depth in the continuous turbulence model is estimated by adding a radioactive tracer at the sea surface that decays with a time scale of 0.5 days^{-1}. The mixed layer depth is defined as the depth where 10% of the surface concentration is found.

by shallow mixing conditions in the beginning of May. The shallow mixing depth persists until beginning of October when the depth of the mixed layer increases rapidly, reaching some 200 m in December. The deepest mixed layer is found in beginning of February.

2.1. A winter mixed layer that is in disequilibrium with the atmosphere

The response of a system that initially is in disequilibrium with the atmosphere is described in Fig. 3. The experiment reflects the case where the initial C_T concentration is 20 μmol/kg below the equilibrium concentration. Further, the influence of the annual cycles in the sea-surface temperature and the biological production on pCO_2^{SW} are neglected in this experiment.

During the first 200 days of integration, the mixed layer depth is generally shallower than 30 m. The air–sea flux of CO_2 is, thus, distributed over a shallow mixed layer, and the C_T concentration increases quickly. The maximum concentration is reached in September–October when the initial disequilibrium has been reduced by 75%. In autumn, the entrainment of water with low total dissolved inor-

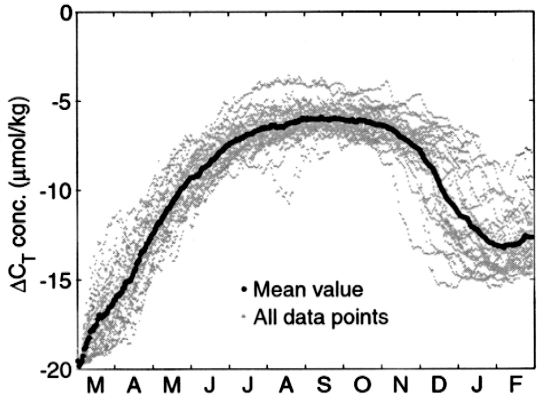

Fig. 3. Some results from a numerical experiment where the total dissolved inorganic carbon concentration initially is 20 μmol/kg below its saturation concentration. In this experiment, the effects from the annual cycles in sea surface temperature and biological production on the partial pressure of CO_2 are not accounted for. The high concentration in summer is the result of the air–sea flux that is trapped in the upper ocean during summer. With a mixed layer depth of 20 m, the equilibration time scale for the upper layer is on the order of 1–2 months, which brings the surface water to be relatively close to equilibrium during summer. In autumn, entrainment brings up water that has not been in contact with the atmosphere and the signal is eroded away.

ganic carbon concentration causes a rapid decrease of the C_T concentration in the upper layer. Thus, at the end of the year, the increase of the C_T concentration in the surface water is 8 μmol/kg (or 40% of the initial signal), although the system was relatively close to equilibrium during summer. The fact that the system is relatively close to equilibrium for an extensive period of time implies that the situation described in Fig. 3 will have a significantly lower flux of atmospheric CO_2 over 1 year as compared to a system where there is deep reaching mixing in the entire period.

2.2. On the influence of the sea-surface temperature cycle

In this experiment, which starts with a total dissolved inorganic carbon concentration that is in equilibrium with the atmosphere, the effect of the temperature on pCO_2^{SW} is included but the biological production is neglected. The magnitude of the SST cycle at station C is on the order of 6°C, which corresponds to a signal of about 100 ppm in pCO_2^{SW}. In this study, I am mainly concerned with the total dissolved inorganic carbon concentration, and it is convenient to introduce an equivalent C_T concentration, defined as the C_T concentration that would produce a similar effect on pCO_2^{SW} as the temperature cycle. The maximum equivalent C_T concentration is on the order of 45 μmol/kg, and its cycle is given in Fig. 4.

When the sea-surface temperature increases, the water is no longer in equilibrium with the atmosphere, and there is an air–sea flux of CO_2 from the upper ocean. The imprint from the air–sea flux is strongest in late September when it is about 25 μmol/kg, or about 50% of the SST signal (Fig. 4). Further, the experiment shows that the signal is strongest when there is a shallow mixed layer. In autumn, water that has not been in contact with the atmosphere is entrained into the upper layer and the signal from the air–sea flux declines. The signal from the air–sea gas exchange is slightly phase-shifted compared to the equivalent SST signal as a result of the slow gas exchange.

The total effect from the SST cycle is defined as the sum of the equivalent C_T concentration and the

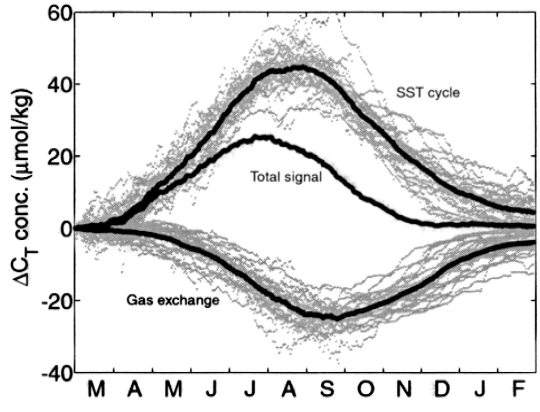

Fig. 4. The influence of the sea surface temperature on the carbon system. The experiment starts with a C_T concentration that is in equilibrium with the atmosphere. Shown in the figure are the annual cycle of the sea surface temperature converted to an equivalent C_T concentration, ΔC_{eqv}, schematically defined as $pCO_2^{SW}\ (T^W,\ C_{Eq}^0 + \Delta C_{eqv}) = pCO_2^{SW}\ (T^W + \Delta SST,\ C_{Eq}^0)$; the total dissolved inorganic carbon concentration in the surface water induced by the air–sea flux of CO_2; and the total signal from the sea surface temperature. Note that the biological production is not accounted for in this model experiment.

air–sea gas exchange (see Fig. 4) and is about 50% of the signal produced by the SST signal alone. The difference is due to the air–sea flux of CO_2 that counteracts the SST cycle. The mean value of the total signal is about 10 μmol/kg, the actual concentration of the water, however, decreases constantly, and the deficit at the end of the experiment is about 5 μmol/kg.

2.3. On the influence of the biological cycle

The biological production in the upper ocean leaves fingerprints on both the nutrient and carbon cycles. Accordingly, the nutrient signal can be used to estimate the direct effect of the biological production on the carbon cycle. I use the simple nutrient cycle, presented in Fig. 5, that reproduces the most basic features of the nutrient cycles at stations C and M. Note that this cycle describes the net effect from biological production and mixing of nutrients from deeper layers.

The stoichiometric form of the biological tissues that are produced is needed to translate the nutrient cycles in Fig. 5 to its carbon equivalence. However, this ratio is not well known and recent estimates range between $C/N \approx 6.5–10$ (Takahashi et al., 1985a; Anderson and Sarmiento, 1994; Sambrotto and Langdon, 1994; Sambrotto et al., 1993; Kendra et al., 1999). I will use $C/N = 9$, which seems to be appropriate for the northern North Atlantic (Honjo, 1980; Honjo and Manganini, 1993; Broström, 1998; Kendra et al., 1999). Moreover, the $CaCO_3$ formation is generally weak in the northern North Atlantic and is neglected in this study (Peng et al., 1987; Bates et al., 1996). When biological production is based on nitrate, protons are consumed and the total alkalinity concentration, thus, follows the nitrate concentration as $\Delta N/\Delta A_T = 1/-1$ (Brewer and Goldman, 1976).

The strength of the air–sea flux of CO_2 triggered by the biological production is investigated in an experiment where the system is forced with the biological production shown in Fig. 5 but where the influence of the sea-surface temperature on pCO_2^{SW} is neglected. The system is initially in equilibrium with the atmosphere, and the signal from the biological production is displayed in Fig. 6 together with the signal from the air–sea flux of CO_2. Note that the effect from biological production is displayed as an equivalent C_T concentration that includes the effect from alkalinity on pCO_2^{SW}.

The removal of total dissolved inorganic carbon from the upper ocean implies that the system becomes undersaturated in summer. The imposed air–sea flux in the experiment is seawards, and its imprint on the ocean has a maximum value in early September (Fig. 6). Again, the shallow mixed layer in the summer implies that the signal from the

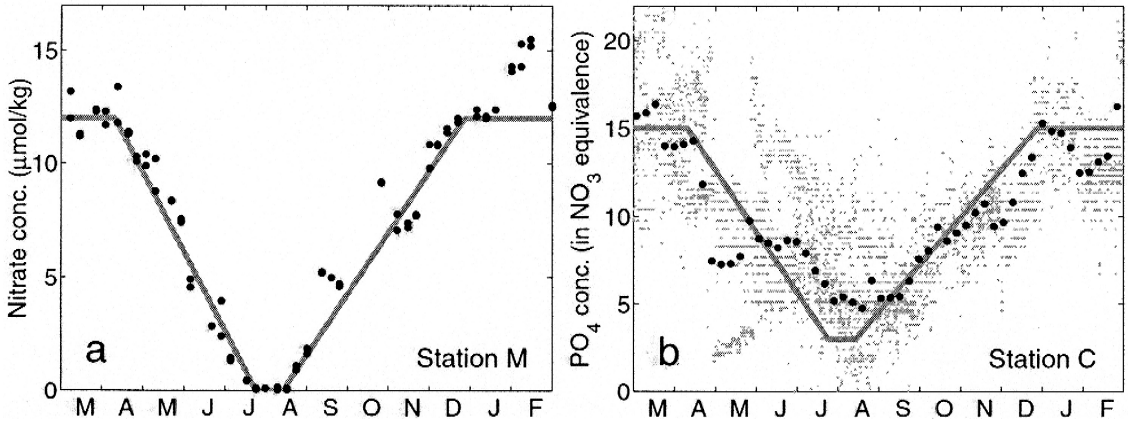

Fig. 5. The nutrient cycles at OWS M (nitrate) and C (phosphate). Note that the phosphate concentration has been multiplied by 16 to be displayed as the nitrate equivalence. The black dots in (b) are the weekly mean of all available data (gray dots). The gray line represents the simple nitrate cycle that is used in this study.

air–sea flux is able to reduce the disequilibrium, created by the biological production, by a significant amount. In autumn, the signals from biological production and the gas exchange decrease with the entrainment of deep water.

2.4. The effect of advection

The effect from advection is described by an experiment where the horizontal advection is parameterized in the form of a constant sink term with strength $u_H \cdot \nabla_H C_T = 10$ μmol kg^{-1} year^{-1}. The strength of the advection corresponds to the case where horizontal advection acting over a 500-m-thick layer counteracts an air–sea flux of 5 mol/(m^2 year). At the start of the experiment, the C_T concentration is chosen to be in equilibrium with the atmosphere. Further, I focus on the effect of advection and neglect the effect from the cycles in SST and biological production on pCO_2^{SW}. The results of the experiments are shown in Fig. 7.

Without the gas exchange, the concentration at the end of the year would be -10 μmol/kg; the air–sea exchanges, thus, contribute with about 2.5 μmol kg^{-1} year^{-1}. Further, the concentration decreases slowly in summer from the combined effect of the air–sea exchange and a shallow mixed layer. In autumn, the concentration decreases rapidly with the entrainment of water that has not been affected by the air–sea flux of CO_2.

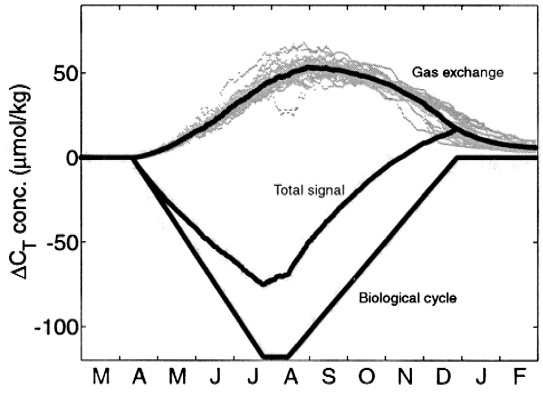

Fig. 6. The signal from the biological production in the upper ocean. The model is initialized to be in equilibrium with the atmosphere; the influence of the sea surface temperature on pCO_2^{SW} is neglected. Shown are the strength of the biological processes; the signal from the induced air–sea flux of CO_2; and the total signal due to the biological production.

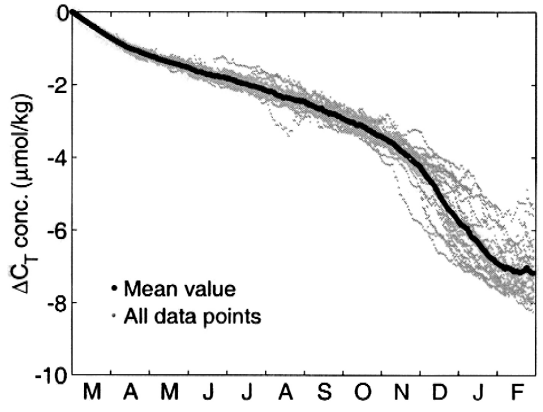

Fig. 7. The influence of the horizontal advection on the annual C_T concentration cycle. The model is initialized with a concentration that is in equilibrium with the atmosphere; the influence of the annual cycles in the sea surface temperature and the biological production on pCO_2^{SW} are neglected. The figure represents the case with $u_H \cdot \nabla_H C_T = 10$ μmol/(kg year).

3. Analyzing the experiments in terms of α and C_{Eq}

To this point, two different formulations of the air–sea flux of CO_2 have been presented: the annually averaged flux described in Eq. (3) and the instantaneous flux described in Eq. (1). The former flux is defined as the annual average of the latter flux:

$$F = \frac{1}{T}\int_0^T F_I(t)\,dt. \qquad (5)$$

Accordingly, to derive Eqs. (3) and (4) from Eqs. (1) and (2), it is necessary to find the annual average of the experiments discussed in Section 2.

3.1. The magnitude of $k(t)\alpha_{CO_2}(t)$

In the annual integration, $k(t)\alpha_{CO_2}(t)$ acts as a weight of the processes contributing to α and C_{Eq}. The $k(t)\alpha_{CO_2}(t)$ can be calculated from the wind speed and the sea-surface temperature, and its magnitude at the different weather stations is shown in

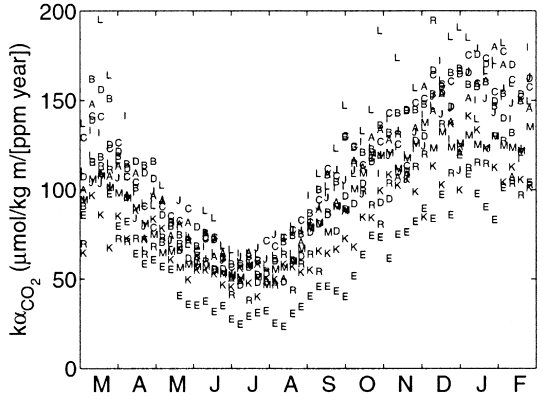

Fig. 8. The weekly mean value of $k(t)\alpha_{CO_2}(t)$ at the OWS. The quantity $k(t)\alpha_{CO_2}(t)$ acts as a weight in the averaging process, thus processes tend to be more important in winter than in summer.

Fig. 8. The $k(t)\alpha_{CO_2}(t)$ follows the wind speed and is highest in the winter months when it reaches above 150 (μmol/kg m)/(ppm year), whereas it is about 50–80 (μmol/kg m)/(ppm year) in summer. Further, its strength is somewhat lower at the southernmost stations C and E than at the other stations. Using the Liss and Merlivat (1986) formulation for the air–sea gas exchange coefficient, the value of $k(t)\alpha_{CO_2}(t)$ would be approximately 70% of those in Fig. 8.

The annual average of a quantity, weighed according to $k(t)\alpha_{CO_2}(t)$, will be investigated in the next sections; the following definition is, thus, useful:

$$\langle x(t)\rangle = \frac{1}{T}\int_0^T k(t)\,\alpha_{CO_2}(t)\,x(t)\mathrm{d}t, \qquad (6)$$

where $\langle\rangle$ denotes the time average, $x(t)$ is an arbitrary function, and $T = 1$ year is the period of integration.

3.2. Defining the parameter α

Let us consider the following relation for α (that may be derived from Eq. (3)):

$$\alpha = \left.\frac{\partial F\left(C_T^W\right)}{\partial C_T^W}\right|_{C_T = C_{Eq}}. \qquad (7)$$

By applying Eq. (5) and using the chain rule:

$$\alpha = \frac{1}{T}\int_0^T \frac{\partial C_T}{\partial C_T^W}\,\frac{\partial pCO_2^{SW}}{\partial C_T}\,\frac{\partial F_I}{\partial pCO_2^{SW}}\bigg|_{C=C_{Eq}}\mathrm{d}t, \qquad (8)$$

F_I depends linearly on pCO_2^{SW} (Eq. (1)); the last part of the expression, thus, evaluates to $k(t)\alpha_{CO_2}(t)$. The middle term may be interpreted as the linearization constant describing how pCO_2^{SW} changes with variations in C_T: I denote this parameter:

$$a_{C_T} = \left.\frac{\partial pCO_2^{SW}}{\partial C_T}\right|_{C_T = C_{Eq}}. \qquad (9)$$

With Eq. (6) and the above statement, Eq. (8) may be written as:

$$\alpha = \left\langle a_{C_T}\left.\frac{\partial C_T}{\partial C_T^W}\right|_{C=C_{Eq}}\right\rangle. \qquad (10)$$

To continue, the total dissolved inorganic carbon concentration is written:

$$C_T = C_T^W + \Delta C_T^{G-W}\left(C_T^W\right) + \Delta C, \qquad (11)$$

ΔC_T^{G-W} reflects the air–sea exchange of CO_2 that is related to the disequilibrium of the winter mixed layer and depends on C_T^W; the last term, ΔC, includes the signal from all other processes. By using Eq. (11), the relation in Eq. (10) becomes:

$$\alpha = \left\langle a_{C_T}\left(1 + \left.\frac{\partial \Delta C_T^{G-W}}{\partial C_T^W}\right|_{C=C_{Eq}}\right)\right\rangle. \qquad (12)$$

With the assumption that the system can be described in linear terms, it is possible to write $\Delta C_T^{G-W} = \Delta C_T^W f(t)$ where $f(t)$ may be estimated from the experiments of Section 2 (note that $f(t)$ is negative). Eq. (12) becomes:

$$\alpha = a_{C_T}\langle 1 + f(t)\rangle. \qquad (13)$$

Eq. (13) implies that α is related to the linearization constant for pCO_2^{SW} vs. C_T multiplied with the annual average (weighed with $k(t)\alpha_{CO_2}$) of the normalized C_T concentration in the surface water $\langle 1 + f(t)\rangle$. Notably, $f(t)$ is a function of the gas exchange and the depth over which the exchanged carbon is distributed.

To evaluate $\langle 1+f(t)\rangle$, I use the experiment displayed in Fig. 3 and the corresponding experiments for the other OWS in the North Atlantic. However, in these experiments, there is a net increase in the C_T concentration over the year. In nature, this net increase is generally compensated by the effect from the horizontal advection. Accordingly, a direct analysis of the model results presented in Fig. 3 may, thus, be misleading, and an artificial component may be introduced that is not present in the natural system where advection counteracts the effect of the air–sea flux. The effect from horizontal advection is, thus, included such that there is no net increase of C_T in the surface water over the annual cycle in any of the analyses.

The estimated magnitudes on $\langle 1\rangle$, $\langle 1+f(t)\rangle/\langle 1\rangle$, and a_{C_T} for the OWS stations are presented in Table 1, and the values of α are visualized in Fig. 9a. Notably, the values of a_{C_T} and $\langle 1+f(t)\rangle$ are such that α is very close to the annual average of the quantity $k(t)\alpha_{CO_2}(t)$. A further discussion on α is left to Section 3.4.

3.3. An evaluation of C_{Eq}

Recalling from Eq. (4), C_{Eq} may be written as:

$$C_{Eq} = C^0_{Eq} + \Delta C^{SST}_{Eq} + \Delta C^{Biol}_{Eq},$$

where C^0_{Eq} reflects the basic state of the ocean; ΔC^{SST}_{Eq} is the correction of the annual SST cycle on the dynamic equilibrium concentration; and ΔC^{Biol}_{Eq} reflects the integrated signal from the biological production.

3.3.1. The definition of the basic state

The basic state of the ocean is defined from the relation:

$$\langle\, pCO_2^W\left(T^W, S^W, C^0_{Eq}, A^W_T\right)\rangle = \langle\, pCO_2^A(t)\rangle, \quad (14)$$

which reflects the concentration, C^0_{Eq}, that would be in equilibrium with the atmosphere in the absence of annual cycles. On an annual time scale, the variability in the atmospheric pCO_2 is small; further, it can readily be evaluated from atmospheric measurements at different locations (Conway et al., 1994; Keeling et al., 1996; Keeling and Shertz, 1992). For station M, the following approximate formula for the atmospheric pCO_2 applies:

$$pCO_2^A(t) = 336.2 + 1.6t' + 0.72\cos(2\pi t') + 6.1\sin(2\pi t') + 0.98\cos(4\pi t') - 1.7\sin(4\pi t'), \quad (15)$$

where $t' = t - 1979$ is given in years (Drange, 1994). With this formula — $\langle\, pCO_2^A(t)\rangle \approx 341$ ppm for 1981 — this is close to the arithmetic mean value of pCO_2^A.

3.3.2. The influence of the annual SST cycle on the dynamic equilibrium concentration

To evaluate the magnitude of ΔC^{SST}_{Eq} from the experiments in Section 2, I assume that the basic relation of Eq. (5) holds for the processes that depend on the SST cycle. Combining Eqs. (1), (5) and

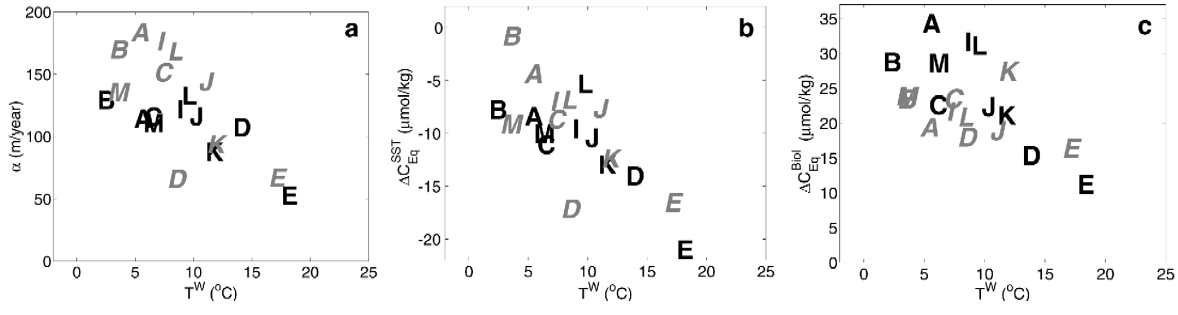

Fig. 9. The estimates of α, ΔC^{SST}_{Eq}, and ΔC^{Biol}_{Eq} for the OWS. The black letters represent the estimate of the data analysis at each station, and the gray italic letters are estimates from the MIT ocean model; see Section 3.4 for details.

(6) gives the following schematic formula for the SST signal:

$$-\alpha\Delta C_{\mathrm{Eq}}^{\mathrm{SST}} = \langle\, p\mathrm{CO}_2^{\mathrm{SW}}\left(\Delta C_{\mathrm{T}}^{\mathrm{SST}}\right)\rangle, \tag{16}$$

where $\Delta C_{\mathrm{T}}^{\mathrm{SST}}$ is the total signal resulting from the SST cycle (i.e., the calculated equivalent C_{T} concentration plus the effect from the gas exchange; see Fig. 4). The changes in the partial pressure due to the changes in the total dissolved inorganic carbon concentration is described using a Taylor expansion of $p\mathrm{CO}_2^{\mathrm{SW}}$:

$$p\mathrm{CO}_2^{\mathrm{SW}}\left(\Delta C_{\mathrm{T}}^{\mathrm{SST}}\right) \approx \frac{\partial p\mathrm{CO}_2^{\mathrm{SW}}}{\partial C_{\mathrm{T}}}\Delta C_{\mathrm{T}}^{\mathrm{SST}}. \tag{17}$$

Using Eqs. (9) and (17) and the formula for α (Eq. (13)), Eq. (16) becomes:

$$\Delta C_{\mathrm{Eq}}^{\mathrm{SST}} = -\frac{\langle \Delta C_{\mathrm{T}}^{\mathrm{SST}}\rangle}{\langle 1+f(t)\rangle}. \tag{18}$$

It should be noted that I use the curve in Fig. 4 that is labeled as the total effect of the SST cycle. The net decrease in C_{T} over a year is compensated by including and adjusting the horizontal advection before doing the analysis. The results from the calculation are reported in Table 1 and in Fig. 9b.

3.3.3. The influence of the biological production on the dynamic equilibrium concentration

$\Delta C_{\mathrm{Eq}}^{\mathrm{Biol}}$ describes the effect from biological production. A similar procedure as for the SST cycle gives:

$$\Delta C_{\mathrm{Eq}}^{\mathrm{Biol}} = -\frac{\langle \Delta C_{\mathrm{T}}^{\mathrm{Biol}}\rangle}{\langle 1+f(t)\rangle}, \tag{19}$$

where $\Delta C_{\mathrm{T}}^{\mathrm{Biol}}$ refers to the total effect of the biological cycle as defined in Fig. 6. Again, I use the horizontal advection to correct the signal such that there is no net increase of total dissolved inorganic carbon concentration in the surface waters over the year. The values of $\Delta C_{\mathrm{Eq}}^{\mathrm{Biol}}$ are calculated using a biological signal corresponding to a nitrate cycle of 12 μmol/kg. However, the initial nutrient concentration changes with location; therefore, the magnitude of the biological cycle is presented as normalized with the initial nutrient concentration in Table 1 (i.e., the results from the analysis is divided with 12 μmol/kg, which is the prescribed strength of the nitrate cycle). The results on $\Delta C_{\mathrm{T}}^{\mathrm{Biol}}$ from this data analysis (where the nitrate concentration at each OWS is taken from the MIT biogeochemical ocean model) are displayed in Fig. 9c together with some results from the MIT biogeochemical ocean model (see Section 3.4).

3.4. The predictions from a biogeochemical ocean model

The estimates on α, $\Delta C_{\mathrm{Eq}}^{\mathrm{SST}}$ and $\Delta C_{\mathrm{Eq}}^{\mathrm{Biol}}$ are displayed in Fig. 9. The figure also shows some results from the MIT biogeochemical ocean model. The MIT ocean model use a finite difference scheme to describe the hydrodynamical equations that characterize the ocean dynamics (Marshall et al., 1997a,b). Small-scale turbulence is represented by a constant turbulent exchange coefficient, and the large-scale ocean eddies are described by an eddy transfer scheme (Gent and McWilliams, 1990; Gent et al., 1995; Visbeck et al., 1997).

The model is used in an off-line mode to simulate the fields for nitrate and total dissolved inorganic carbon. The biological processes are simulated with a nitrate dependent removal of nitrate and carbon from the upper layer. Although this represents a very crude description of the biological processes in the upper ocean, the model mimics the annual cycles relatively well (the production tends to start somewhat late and the productive season is slightly too long). The carbon chemistry is similar to the model described in Follows et al. (1996), but here a C/N ratio = 9 for production is used.

The values of $\Delta C_{\mathrm{Eq}}^{0}$, $\Delta C_{\mathrm{Eq}}^{\mathrm{SST}}$, and $\Delta C_{\mathrm{Eq}}^{\mathrm{Biol}}$ that are representative for the model are found from some idealized experiments where the advection for total dissolved inorganic carbon is turned off. Moreover, the model experiments are integrated until a repeating annual cycle is reached (i.e., the dynamic state where the integrated effect of the annual cycle is in equilibrium with the atmosphere). This experiment is considered for three different scenarios: (i) the case with $p\mathrm{CO}_2^{\mathrm{SW}} = p\mathrm{CO}_2^{\mathrm{SW}}(T^{\mathrm{W}}, C_{\mathrm{T}})$ (i.e., the partial pressure of CO_2 in the water is calculated using the temperature of the winter mixed layer and where the biological production is not considered); (ii) the case

with an annual cycle in temperature but no biological cycle (i.e., $pCO_2^{SW} = pCO_2^{SW}(T, C_T)$); (iii) the last experiment reflects the case with annual cycles of both sea-surface temperature and biological production, thus, $pCO_2^{SW} = pCO_2^{SW}$ $(T, C_T + \text{Biol})$. The values of ΔC_{Eq}^{0}, ΔC_{Eq}^{SST}, and ΔC_{Eq}^{Biol} are found by comparing the C_T in the winter water between these experiments. The model results are extracted at the positions of the OWS and shown in Fig. 9.

The model predictions on C_T^W, C_{Eq}, and F from the MIT ocean model experiments may be used to calculate α from Eq. (3). The estimates on α from the data analysis and the MIT ocean model are shown in Fig. 9a. There is a clear trend that the value of α is small at high temperatures and stronger at low temperatures. This is the result of weak wind speeds as well as small values of a_{C_T} at high temperatures. Although there are some scatters in the estimates, there is generally a good agreement between values from the data analysis and the estimates from the MIT ocean model. For stations A, I, and L, the MIT biogeochemical model predicts values on α that is close to the theoretical limit where the air–sea flux of CO_2 plays no role for the exchange dynamics. However, the advection is strong in these areas; thus, it is possible that the advection is important for the air–sea flux on time scales shorter than the annual cycle. To reveal whether this is a realistic result or not, a comprehensive analysis of the result from the MIT biogeochemical model must be completed.

The estimate of ΔC_{Eq}^{SST} as a function of the temperature is displayed in Fig. 9b. The magnitude of ΔC_{Eq}^{SST} is small at cold temperatures, about -5 to -10 μmol/kg at say 6°C, and it is about -20 μmol/kg in the southern North Atlantic. These changes in ΔC_{Eq}^{SST} cannot be attributed to a single mechanism; instead, it is the combined effect from long summer periods with high temperature at the southernmost stations, stronger temperature cycles, lower gas exchange coefficients, and the way pCO_2^{SW} depends on the temperature and the C_T concentration. Notably, there is a good conformity between the analysis of the OWS data as rendered from the data analysis and the results from the MIT ocean model supporting the method developed in this study.

The effect from the biological cycle is strongest in the northern North Atlantic. Given the simple biological production function used in this study, the changes in ΔC_{Eq}^{Biol} between the stations in Fig. 9c are essentially due to high nutrient concentrations at high altitudes. The results from the data analysis are in fair agreement with the results from the MIT ocean model. The discrepancy may partly be due to the fact that the biological processes in the one-dimensional model and the MIT ocean model are described in simple but, nevertheless, different ways.

In the MIT biogeochemical model, the biological drawdown of nutrients is not strong enough in spring–summer whereas it tends to be too strong in autumn. For the simple model in the data analysis, I use a prescribed nutrient cycle. Although it fits observations from stations C and M, it will not adjust in a proper way to the different mixing and biological conditions that most likely exist at other stations. Accordingly, the formulation does not describe the long productive seasons in the southern regions and the short productive seasons in the northwestern regions. Thus, I expect that the value from the data analysis on ΔC_{Eq}^{Biol} for stations C and M are reliable. However, the data analysis may give too high values in the northwestern region of the North Atlantic — which have shorter periods with weak mixing — and too low values in the southern regions that have long periods with weak mixing.

4. An estimate of the air–sea flux of CO_2 for the North Atlantic

It is necessary to know the spatial distribution of α as well as the fields for C_T^W and C_{Eq} to estimate air–sea flux of CO_2 in the North Atlantic (note that the T^W, A_T^W, and NO_3^W fields are needed to calculate C_{Eq}). The properties of the winter mixed layer are estimated from the TTO/NAS expedition that covered the main part of the North Atlantic from April to September, 1981 (Brewer et al., 1986). I use the mean value of the measurements between 80 and 200 m depth to extract the properties of the winter mixed layer from the measurements taken in summer. This layer is well below the influence of the summer mixed layer and generally above the bottom of the winter mixed layer. Ideally, this layer, thus, acts as a memory of the winter mixed layer (Glover

and Brewer, 1988). The estimated fields for T^{W}, C_{T}^{W}, A_{T}^{W}, and NO_{3}^{W} are displayed in Fig. 10.

The equilibrium concentration is calculated from T^{W}, A_{T}^{W}, and NO_{3}^{W} using Eq. (4). To evaluate the strength of the annual cycles at different positions in the North Atlantic, I use $\Delta C_{Eq}^{SST} = -(T^{W} + 2)$ μmol/kg in accordance with Fig. 9b; the number 2 is used to avoid negative values near the freezing point. Further, I assume that $\Delta C_{Eq}^{Biol} = 2.5 \cdot NO_{3}^{W}$ μmol/kg (Table 1) and $\alpha = 160 - 4(T^{W} + 2)$ μm/year based on its relation with the temperature shown in Fig. 10a.

The air–sea flux of CO_2 is estimated for each individual station and the result is displayed in Fig. 11a. The flux predicted by the MIT biogeochemical ocean model is shown in Fig. 11b. Comparing the two estimates, they both predict that the air–sea flux of CO_2 is most intense in the Nordic Seas and in the Labrador Sea. These regions are characterized by strong heat fluxes that produce water that is undersaturated with respect to CO_2. Off the Grand Banks, however, there is an area where the air–sea flux of CO_2 is somewhat lower. The area is clearly seen in the model results, and it can be seen in the analysis of the TTO/NAS data.

The main deviation between the two estimates is along the North American coast at 40–50°N. The MIT model predicts that there is an intensive air–sea flux of CO_2 in this area whereas the data analysis hints that the flux is of the opposite sign. The misfit

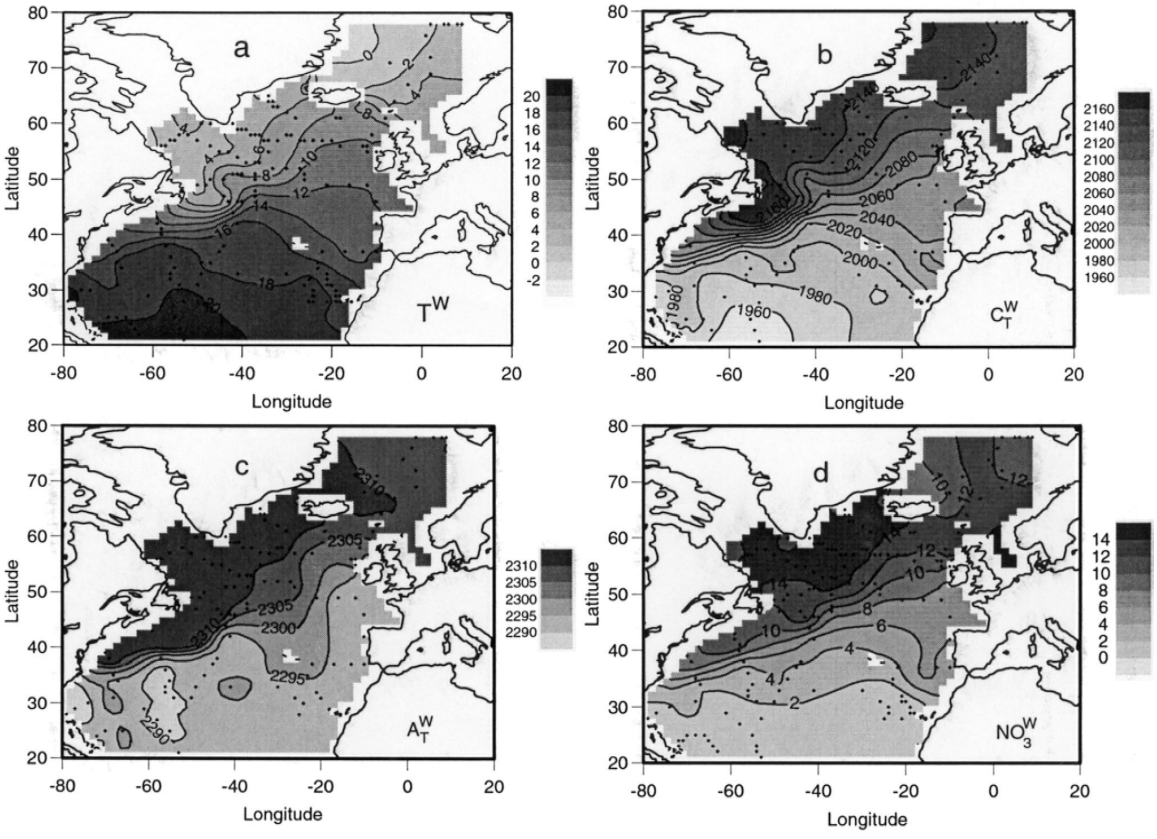

Fig. 10. The properties of the winter mixed layer in the North Atlantic: (a) temperature; the concentrations of (b) total dissolved inorganic carbon, (c) total alkalinity, and (d) nitrate. Data are taken from the TTO/NAS expedition (Brewer et al., 1986). The winter mixed layer concentrations are estimated from summer measurements by taking the mean of the measurements between 80 and 200 m, which is below the bottom of the summer mixed layer and above the bottom of the winter mixed layer. The total dissolved inorganic carbon and total alkalinity concentrations have been normalized to 35 psu.

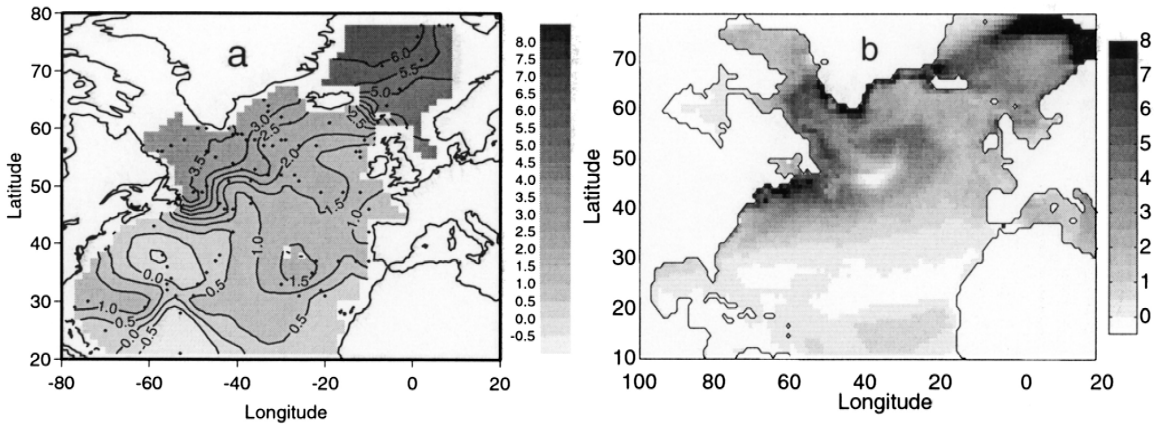

Fig. 11. Estimates of the air–sea flux of CO_2, units are in mol/(m^2 year) (a) using data from the TTO/NAS expedition and (b) the results from the MIT ocean model.

between the two estimates is most likely a combination of too strong forcing (and too northward flowing Gulf Stream) in the ocean model, and an overestimate of the Labrador Sea water in the data analysis. Moreover, the estimate from the data analysis shows a rather large flux in the eastern part of the North Atlantic that is not present in the model estimate. There are, however, only a few data points from the TTO/NAS expedition in this region, so the flux predicted from these data should be viewed with some caution.

The zonal integrated fluxes from the two estimates are shown in Fig. 12. In the northern part of the region — where there is good data coverage — the two estimates give similar results. Nevertheless, the estimated flux is somewhat lower than the modeled flux. One reason may be that the data analyses do not show any strong flux at the boundary currents along the Greenland and the North America (probably because the fact that there are few stations close to the coast in the TTO/NAS dataset), this boundary current clearly shows up in the model results. At 40–50°N, the MIT ocean model predicts that there is a peak in the air–sea flux that is not present in the estimate based on the TTO/NAS data. The main reason is the deviations in the predicted fluxes at the North American coast. Further to the south, the two estimates also give somewhat different results. In this region, the data coverage is sparse and the estimate of the flux from the data analysis may have large uncertainties.

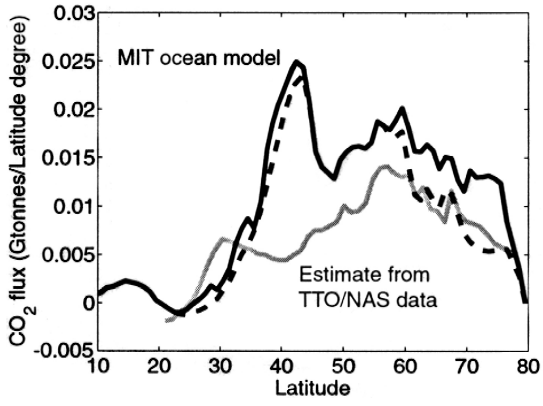

Fig. 12. A zonal integration of the fluxes presented in Fig. 11. The two curves for the MIT biogeochemical model are: a solid line — the flux for the entire model area, and a dashed line — the fluxes from the area that correspond to the area of the data analysis.

5. Discussion

In this study, I focus on the air–sea flux of CO_2 and specifically the role the annual cycles may have for the flux. The influence of the annual cycles may be divided into two parts. The direct effect of the sea-surface temperature and the biological production on pCO_2^{SW} is easily evaluated from measurements. The second part reflects how the air–sea flux

is distributed in the upper ocean during the annual cycle. If the air–sea flux is distributed over a shallow depth, the C_T concentration in the surface layer will change rapidly and affect the air–sea flux later in the season. It is essential to have precise knowledge of the mixing properties in the upper ocean and its time evolution to evaluate this part of the system.

The influences of the annual cycles are investigated through a number of model experiments where each process that is important for the carbon system is investigated separately (see Figs. 3–7). The sum of all these experiments represent an annual cycle that may be compared with measurements (see Fig. 13). The model results are obtained by superposing the results from the experiments shown in Figs. 3–7, where the strength of the horizontal advection are adjusted such that the initial surface water concentrations are reached at the end of the year.

According to the model, the form of the annual signals at stations C and M are dominated by the biological activity that creates low C_T concentrations in the surface water during summer. In autumn, the entrainment of deep water with high dissolved inorganic carbon concentration leads to an increase in the C_T concentration. There are significant scatters in the data, but the main features of the data are well reproduced by the model. It may be noticed that the model slightly overestimates the C_T concentration in summer despite the fact that the biological material is described by a C/N ratio = 9. Accordingly, there are some indications that the gas exchange formulation in the model (Wanninkhof, 1992) is somewhat high (cf. Liss and Merlivat, 1986; Woolf and Thorpe, 1991; Wanninkhof, 1992) or that the C/N ratio of the produced organic material exceeds nine. Observations from the upper waters of the northern North Atlantic often show large amounts of dissolved organic carbon (DOC) (Chen et al., 1996; Børsheim and Myklestad, 1997). Accordingly, if DOC with a high C/N ratio were to be included in the model, it would produce results that are more consistent with measurements (Broström, 1998).

The long time scale for the exchange of CO_2, which generally is longer than 1 year, implies that the integral effect of the annual cycles must be considered when estimating the dynamic equilibrium state of the system. An integration of the SST cycle shows that its contribution to the dynamic equilibrium concentration is strongest in the warm southern areas — with an influence of about −15 μmol/kg

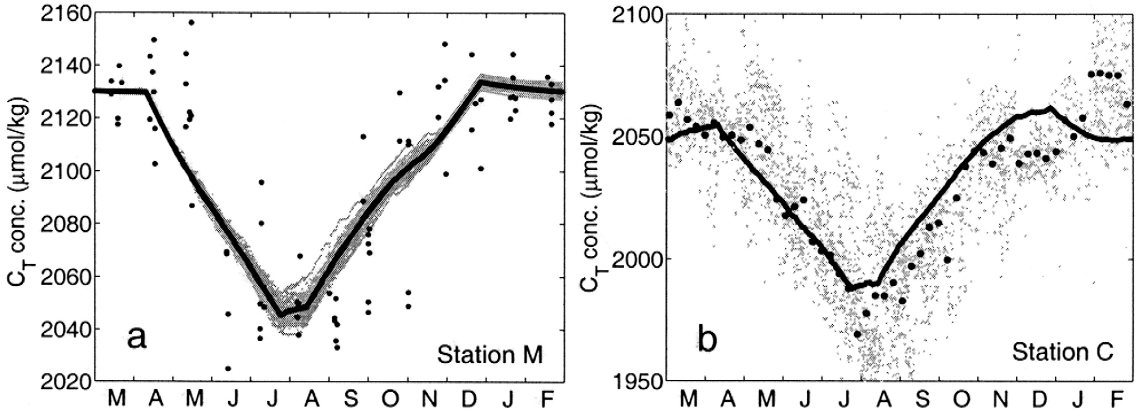

Fig. 13. A comparison of the estimated total inorganic carbon concentration with data. (a) For station M (Gislefoss et al., 1998), and (b) for station C. For station M, I assume that the surface water initially is in equilibrium with the atmosphere (Gislefoss et al., 1998), whereas for station C, the winter water is taken to be undersaturated with 20 μmol/kg in C_T. The total dissolved inorganic carbon concentrations presented for station C have been calculated from pH measurements and an estimate of the total alkalinity concentration (Peng et al., 1987), i.e., the $CaCO_3$ production is neglected, which implies that A_T follows the nitrate concentration (Brewer and Goldman, 1976). The gray dots represent all data, and the black dots are the weekly mean of the gray dots. The total dissolved inorganic carbon concentration has been normalized to 35 psu.

on the dynamic equilibrium concentration — whereas its influence is relatively weak in the northern areas. The signal from the biological cycle to some extent follows the nutrient availability, but the length of the productive season is most likely also important. The biological production contributes with about 30 μmol/kg to the dynamic equilibrium concentration in the northern nutrient rich parts, whereas it has only a minor influence in the southern nutrient depleted areas.

From Fig. 10b, I conclude that the difference in C_T^W concentration between the northern and southern North Atlantic is about 200 μmol/kg. If nitrate is used as a proxy for the combination of advection and mixing, it may be concluded that advection/mixing explains about 100 μmol/kg of this difference (as calculated from the north–south difference in nitrate concentration, which is 12 μmol/kg, and a C/N ratio of 9). Thus, 100 μmol/kg should be the result of the air–sea exchange of CO_2 driven by changes in the dynamic equilibrium concentration between the northern and southern North Atlantic. The net effect of the annual cycle between these areas, as described by $\Delta C_{Eq}^{SST} + \Delta C_{Eq}^{Biol}$, is on the order of 40 μmol/kg. This is a significant part of the dynamical difference (or difference due to air–sea gas exchange) between the southern and the northern North Atlantic. Thus, the annual cycles in sea-surface temperature and biological production are important to account for in any simulation of the carbon cycle.

The air–sea flux of CO_2 can be calculated if the basic state of the ocean (i.e., the temperature and the total alkalinity concentration) is known and if the net effect of the annual cycle can be expressed. The impact of the SST cycles on the equilibrium may be found from data from the OWS, for example; and the nitrate concentration in winter gives a first order estimate of the strength of the biological production. Data from the TTO/NAS expedition are used to find the winter state in the North Atlantic and the air–sea flux of CO_2 (estimated for 1981) is essentially 0.4 Gt C/year for the area north of 30°N. This is somewhat lower than the estimate from the MIT biogeochemical model but is similar to other estimates of the air–sea flux for the area (Takahashi et al., 1993; Watson et al., 1995). The spatial and zonal integrated flux calculated from data generally show good agreement with the air–sea flux estimates from the MIT ocean model. I find that the fluxes are high in the Nordic Seas and the Labrador Sea, areas that are known to have an intensive air–sea heat flux — a feature that is strongly coupled to the flux of CO_2 (Takahashi et al., 1993; Watson et al., 1995).

The framework presented in this study works exceptionally well for the North Atlantic. A network of OWS permits a thorough analysis of the upper ocean dynamics. Further, the North Atlantic is characterized by very deep mixing in winter; this resets the upper ocean concentrations such that that the annual cycles more or less originates from a clean state. However, it seems reasonable that the framework presented in this study can be extended to describe the general features in mid to high latitude dynamics of the North Pacific and the southern ocean.

Acknowledgements

I would like to thank Prof. Gösta Walin for many discussions on the dynamics of the carbon system. Mick Follows introduced me to the MIT biogeochemical ocean model and gave some helpful comments on an early version of the manuscript. Three anonymous reviewers also contributed with helpful comments. The work is a part of a Scandinavian project, sponsored by the Nordic Council of Ministers, that investigates the flux of carbon dioxide in the Greenland–Iceland–Norwegian Sea. I am also thankful to the Knut and Alice Wallenberg foundation that sponsored a postdoctoral fellowship to MIT.

Appendix A. Mixing model

In this appendix, the model for the turbulent mixing in the upper ocean is described.

A.1. Basic equations

I consider a one-dimensional model where the turbulent mixing is described according to the eddy viscosity concept (Rodi, 1980, 1987). With this as-

sumption, the conservation equations for momentum, heat and salt are:

$$\frac{\partial u}{\partial t} - fv = \frac{\partial}{\partial z}\left[\nu_t \frac{\partial u}{\partial z}\right], \tag{A1a}$$

$$\frac{\partial v}{\partial t} + fu = \frac{\partial}{\partial z}\left[\nu_t \frac{\partial v}{\partial z}\right], \tag{A1b}$$

$$\frac{\partial T}{\partial t} = \frac{\partial}{\partial z}\left[\nu_t \frac{\partial T}{\partial z}\right] + \frac{1}{c_p \rho}\frac{\partial I}{\partial z} + Q_{\ln}, \tag{A1c}$$

$$\frac{\partial S}{\partial t} = \frac{\partial}{\partial z}\left[\nu_t \frac{\partial S}{\partial z}\right], \tag{A1d}$$

where u and v are the velocity components in the x and y direction, respectively; ν_t is the eddy viscosity (the same for all variables except k and ε as described later); f is the Coriolis parameter; T and S are temperature and salinity; I is the solar radiation in the water; ρ is the density of water; c_p is the specific heat of water; and $Q_{\ln}$ is an internal heat source interpreted as large-scale advection in combination with a temperature gradient. $Q_{\ln}$ is fitted toward observations at each station (Broström, 2000).

About 50% of the solar radiation that penetrates the sea surface is infrared radiation that is trapped within the uppermost few centimeters. The remaining radiation is distributed in the ocean as

$$\frac{\partial I}{\partial z} = kI, \tag{A2}$$

where k is the extinction coefficient for sea water. The radiation at the surface is given as:

$$I(z=0) = 0.5 Q_{SW}, \tag{A3}$$

where Q_{SW} is the solar radiation at the sea surface.

A.2. Boundary and initial conditions

The boundary conditions to Eqs. (A1a–d) are:

$$\nu_t\left[\frac{\partial u}{\partial z}, \frac{\partial v}{\partial z}, \frac{\partial T}{\partial z}, \frac{\partial S}{\partial z}\right] = \left[\frac{\tau_x}{\rho}, \frac{\tau_y}{\rho}, \frac{Q}{c_p \rho}, S(E-P)\right]$$

at $z = 0$, (A4a–d)

and:

$$\nu_t\left[\frac{\partial u}{\partial z}, \frac{\partial v}{\partial z}, \frac{\partial T}{\partial z}, \frac{\partial S}{\partial z}\right] = 0 \qquad \text{at } z = -H, \quad \text{(A4e–h)}$$

where $-H$ is the bottom of the model domain. (τ_x, τ_y) is the wind stress vector, which is calculated from the wind at 10 m height (Large and Pond, 1981). $E-P$ is the net evaporation; in this study $E-P=0$ is used.

Q is the heat flux at the sea surface given as:

$$Q = Q_{SW} - Q_{LW} - Q_S - Q_L. \tag{A5}$$

Q_{SW} is the solar radiation, Q_{LW} the long wave radiation, and Q_S, Q_L are the sensible and latent heat fluxes. A set of heat flux parameterizations that are consistent with the thermal cycles at the OWS stations are given in Broström (2000). The boundary conditions in Eqs. (A4a–A5) are calculated from observations on the wind speed, air temperature, humidity, wind speed, and cloudiness that were taken every 3 h at each OWS. I only consider years when there is a complete coverage in the observations.

The initial conditions for temperature and salinity are taken from the interpolated NODC data set. The temperature in the uppermost part of the ocean, however, has been corrected to reproduce the observed sea-surface temperature in the initial part of the integration.

A.3. Turbulence model

The turbulent diffusion coefficient is the sum of two distinctive parts: (i) turbulence driven by shear/buoyancy production of turbulent kinetic energy, ν_S; and (ii) turbulence arising from wave action, ν_w. Thus, the total turbulent exchange coefficient is given as:

$$\nu_t = \nu_S + \nu_w. \tag{A6}$$

Shear driven turbulence models often generate a very weak transport of momentum through stable density gradients (Ayotte et al., 1996; Large et al., 1994). Thus, the shear/buoyancy-produced turbulence generally dominates in the upper part of the ocean and

down to where density gradients become large. Below this region, the shear-produced turbulence is weak and wave action is the dominant source of turbulent kinetic energy. To simulate the mixing by waves and the effect from subduction in the upper ocean, I use:

$$\nu_w = \left(1 \times 10^{-5} + 9 \times 10^{-5} \exp(-(z-30)/30)\right). \quad \text{(A7)}$$

The k–ε model (Rodi, 1980, 1987) is used to describe the turbulence mixing forced by shear/buoyancy production of turbulent kinetic energy. Variables in the k–ε model are the turbulent kinetic energy, k, and its dissipation rate, ε, where ν_S is related to these. The equations for the turbulent kinetic energy follow from a straightforward derivation found in general textbooks on fluid mechanics. The equation for the dissipation rate is more uncertain and is generally considered to have a highly parameterized form. The model equations are:

$$\frac{\partial k}{\partial t} = \frac{\partial}{\partial z}\left[\frac{\nu_t}{\sigma_k}\frac{\partial k}{\partial z}\right] + P_S + P_B - \varepsilon, \quad \text{(A8a)}$$

$$\frac{\partial \varepsilon}{\partial t} = \frac{\partial}{\partial z}\left[\frac{\nu_t}{\sigma_\varepsilon}\frac{\partial \varepsilon}{\partial z}\right] + \frac{\varepsilon}{k}\left(C_{1\varepsilon}P_S + C_{3\varepsilon}P_B - C_{2\varepsilon}\varepsilon\right), \quad \text{(A8b)}$$

$$\nu_S = C_\mu \frac{k^2}{\varepsilon}, \quad \text{(A8c)}$$

where:

$$P_S = \nu_t\left[\left(\frac{\partial u}{\partial z}\right)^2 + \left(\frac{\partial v}{\partial z}\right)^2\right], \quad \text{(A8d)}$$

$$P_B = \nu_t g\left[-\alpha\frac{\partial T}{\partial z} + \beta\frac{\partial S}{\partial z}\right]. \quad \text{(A8e)}$$

C_μ, $C_{1\varepsilon}$, $C_{2\varepsilon}$, $C_{3\varepsilon}$, σ_k, and σ_ε are empirical constants in the model (Rodi, 1980); g is gravity; P_S is the production of turbulence due to shear; P_B is the production or destruction due to buoyancy effects. Finally, α and β are constants in the linearized equation for density:

$$\rho(T,S) = \rho_r\left(1 - \alpha(T - T_r) + \beta(S - S_r)\right), \quad \text{(A9)}$$

Table A1
Numerical values of constants involved in the physical model

Constant	Meaning	Value
C_μ	Constant in turbulence model.	0.09
$C_{1\varepsilon}$	Constant in turbulence model.	1.44
$C_{2\varepsilon}$	Constant in turbulence model.	1.92
$C_{3\varepsilon}$	Constant in turbulence model.	0.8
σ_k	Prandtl/Schmidt number for k.	1.4
σ_ε	Prandtl/Schmidt number for ε	1.3
β	Salinity expansion coefficient.	$8 \cdot 10^{-4}$ psu^{-1}
k	Light extinction coefficient water.	0.1 m^{-1}

where ρ_r and S_r are reference density and salinity (these are taken as constants); α depends on the reference temperature according to:

$$\alpha = 2.14 \times 10^{-4} + 4.5 \times 10^{-6}(T_r - 20), \quad \text{(A10)}$$

where T_r is the reference temperature (i.e., T_r is the mean temperature at each station) and varies with each OWS as given by Table 1. Eq. (A10) is formulated from the second order Taylor expansion term of the UNESCO density formula.

With boundary conditions for k and ε (Rodi, 1980), Eqs. (A1a–10) forms a closed set of equations. The equations are solved using the numerical method implemented in the PROBE routine, developed at the Swedish Meteorological and Hydrological Institute (SMHI); (Svensson, 1986). PROBE uses a finite difference scheme based on an implicit code. Maximum depth is 800 m. The model has 500 grid points; it is nonuniform and has 1-m resolution at the sea surface and about 15 ms at the bottom. The model is stepped forward in time using 300-s time steps. Numerical values of the constants in the physical model are presented in Table A1.

A.4. Carbon model

The equation for the total dissolved inorganic carbon concentration is:

$$\frac{\partial C_T}{\partial t} + u_H \cdot \nabla_H C_T = \frac{\partial}{\partial z}\left[\nu\frac{\partial C_T}{\partial z}\right] + \text{Biol.} \quad \text{(A11)}$$

The effect of the horizontal advection is taken as constant with time and over the entire depth:

$$u_H \cdot \nabla_H C_T = \text{constant}. \quad \text{(A12)}$$

The effect from biological production follows a prescribed nitrate cycle:

$$\mathrm{Biol} = \gamma_{\mathrm{C/N}} \frac{\partial \mathrm{NO_3}}{\partial t}, \qquad \text{(A13)}$$

where $\gamma_{\mathrm{C/N}} = 9$ is the carbon to nitrogen ratio of the biological production. With the prescribed nitrate cycle that I use in this study, it should be noted that the formulation describes the net effect of the biological production and mixing processes. At the sea surface, there is a flux condition for CO_2:

$$\nu_t \frac{\partial C_{\mathrm{T}}}{\partial z} = k\alpha_{\mathrm{CO_2}}\left(p\mathrm{CO_2^{SW}} - p\mathrm{CO_2^{A}}\right), \qquad \text{(A14)}$$

where $k\ \alpha_{\mathrm{CO_2}}$ is the gas exchange coefficient (Wanninkhof, 1992) multiplied by the solubility of CO_2 in sea water (Weiss, 1974). $p\mathrm{CO_2^{SW}}$ and $p\mathrm{CO_2^{A}}$ are the partial pressure of CO_2 in the sea water and the atmosphere, respectively. The partial pressure of CO_2 in the water is generally a function of the temperature, total inorganic carbon, and total alkalinity concentrations in the water, schematically written as $p\mathrm{CO_2^{W}} = p\mathrm{CO_2^{W}}(T, C_{\mathrm{T}}, A_{\mathrm{T}})$. However, in the experiments, I may consider constant values for T and/or the C_{T} and A_{T} concentrations to study the influence of certain processes.

References

Anderson, L.A., Sarmiento, J.L., 1994. Redfield ratios of remineralization determined by nutrient data analysis. Global Biogeochem. Cycles 8, 65–80.

Ayotte, K.W., Sullivan, P.P., Andren, A., Doney, S.C., Holtslag, A.A.M., Large, W.G., McWilliams, J.C., Chin Hoh, M., Otte, M.J., Tribbia, J.J., Wyngaard, J.C., 1996. An evaluation of neutral and convective planetary boundary-layer parameterizations relative to large eddy simulations. Boundary Layer Meteorol. 79, 131–175.

Bates, N.R., Michaels, A.F., Knap, A.H., 1996. Alkalinity changes in the Sargasso Sea: geochemical evidence of calcification? Mar. Chem. 51, 347–358.

Børsheim, K.Y., Myklestad, S.M., 1997. Dynamics of DOC in the Norwegian Sea inferred from monthly profiles collected during three years at 66°N 2°E. Deep-Sea Res. 44, 593–601.

Brewer, P.G., Goldman, J.C., 1976. Alkalinity changes generated by phytoplankton growth. Limnol. Oceanogr. 21, 108–117.

Brewer, P.G., Takahashi, T., William's, R.T., 1986. Transient tracers in the ocean (TTO) — hydrographic data and carbon dioxide systems with revised carbon chemistry data. NDP-004/R1, Carbon Dioxide Information Analysis Center (CDIAC), Oak Ridge National Laboratory, Oak Ridge, TN, USA.

Broecker, W.S., Peng, T.-H., 1982. Tracers in the Sea. Eldigo Press, Lamont-Doherty Geological Observatory, Palisades, NY, 690 pp.

Broström, G., 1997a. Air–sea flux of CO_2 — can we short cut the annual cycle? A Norwegian Sea case study. Phys. Chem. Earth 21, 517–522.

Broström, G., 1997. Interaction between mixed layer dynamics, gas exchange and biological production in the oceanic surface layer with application to the northern North Atlantic. PhD thesis, Göteborg University, Gothenburg, Sweden.

Broström, G., 1998. A note on the C/N and C/P ratio of the biological production in the Nordic Seas. Tellus, Ser. B 50, 93–109.

Broström, G., 2000. A set of heat flux formulations that are consistent with data from the Ocean Weather Stations, (in preparation).

Chen, F.R., Fry, B., Hopkinson, C.S., Repeta, D.J., Peltzer, E.T., 1996. Dissolved organic carbon on Georges Bank. Cont. Shelf Res. 16, 409–420.

Conway, T.J., Tans, P.P., Waterman, L.S., Thoning, K.W., Kitzis, D.R., Masarie, K.A., Zhang, N., 1994. Evidence for interannual variability of the carbon cycle from the National Oceanic and Atmospheric Administration/Climate Monitoring and Diagnostics Laboratory Global Air Sampling Network. J. Geophys. Res. 99, 22831–22855.

Drange, H, 1994. An isopycnic coordinate carbon cycle model for the North Atlantic and the possibility of disposing of fossil fuel CO_2 in the ocean. PhD Thesis, Nansen Environmental and Remote Sensing Centre. Bergen, Norway.

Fan, S., Gloor, M., Mahlman, J., Pacala, S., Sarmiento, J., Takahashi, T., Tans, P., 1998. A large terrestrial carbon sink in North America implied by atmospheric and carbon dioxide data and models. Science 282, 442–446.

Follows, M.J., Williams, R.G., Marshall, J.C., 1996. The solubility pump of carbon in the subtropical gyre of the North Atlantic. J. Mar. Res. 54, 605–630.

Gent, P.R., McWilliams, J.C., 1990. Isopycnal mixing in ocean circulation models. J. Phys. Oceanogr. 20, 150–155.

Gent, P.R., Willebrand, J., McDougall, T.J., McWilliams, J.C., 1995. Parameterizing eddy-induced tracer transports in ocean circulation models. J. Phys. Oceanogr. 25, 463–474.

Gislefoss, J.S., Nydal, R., Slagstad, D., Sonninen, E., Holmén, K., 1998. Carbon time series in the Norwegian Sea. Deep-Sea Res. 45, 433–460.

Glover, D.M., Brewer, P.G., 1988. Estimates of wintertime mixed layer nutrient concentrations in the North Atlantic. Deep-Sea Res. 35, 1525–1546.

Honjo, S., 1980. Material fluxes and modes of sedimentation in the mesopelagic and bathypelagic zones. J. Mar. Res. 38, 53–97.

Honjo, S., Manganini, S.J., 1993. Annual biogenic particle fluxes to the interior of the North Atlantic Ocean; studied at 34°N 21°W and 48°N 21°W. Deep-Sea Res. 40, 587–607.

Keeling, C.D., Whorf, T.P., 1996. Atmospheric CO_2 records from sites in the SIO sampling network: a compendium of data on

global change. Carbon Dioxide Information Analysis Center, Oak Ridge National Laboratory, Oak Ridge, TN, USA.

Keeling, R.F., Piper, S.C., Heimann, M., 1996. Global and hemispheric CO_2 sinks deduced from changes in atmospheric O_2 concentration. Nature 381, 218–221.

Keeling, R.F., Shertz, S.R., 1992. Seasonal and interannual variations in atmospheric oxygen and implications for the global carbon cycle. Nature 358, 723–727.

Kendra, L.D., Wallace, D.W.R. Jr., Wallace, W.O.S., Skoog, A., Lara, R., Gosselin, M., Falck, E., Yager, P.L., 1999. Non-Redfield carbon and nitrogen cycling in the Arctic: effects of ecosystem structure and dynamics. J. Geophys. Res. 104, 3185–3199.

Large, W.G., McWilliams, J.C., Doney, S.C., 1994. Oceanic vertical mixing: a review and a model with a nonlocal boundary layer parameterization. Rev. Geophys. 32, 363–403.

Large, W.G., Pond, S., 1981. Open ocean momentum flux measurements in moderate to strong winds. J. Phys. Oceanogr. 11, 324–336.

Lee, K., Wanninkhof, R., Takahashi, T., Doney, S.C., Feely, R.A., 1998. Low interannual variability in recent oceanic uptake of atmospheric carbon dioxide. Nature 396, 155–159.

Liss, P.S., Merlivat, L., 1996. Air–sea exchange rates: introduction and synthesis. In: Buat-Ménard, P. (Ed.), The Role of Air–Sea Exchange in Geochemical Cycling. NATO ASI Ser., Ser. C D. Riedel Publishing, The Netherlands, pp. 113–127.

Marland, G., Boden, T.A., Andres, R.J., Brenkert, A.L., Johnston, C.A., 1998. Global, regional, and national CO_2 emissions, trends: a compendium of data on global change. Carbon Dioxide Information Analysis Center, Oak Ridge National Laboratory, Oak Ridge, TN, USA.

Marshall, J., Adcroft, A., Hill, C., Perelman, L., Heisey, C., 1997a. A finite-volume, incompressible Navier Stokes model for studies of the ocean on parallel computers. J. Geophys. Res. 102, 5753–5766.

Marshall, J., Hill, C., Perelman, L., Adcroft, A., 1997b. Hydrostatic, quasi-hydrostatic, and nonhydrostatic ocean modeling. J. Geophys. Res. 102, 5733–5752.

Peng, T.-H., Takahashi, T., Broecker, W.S., Olafsson, J., 1987. Seasonal variability of carbon dioxide, nutrients and oxygen in the northern North Atlantic surface water: observations and a model. Tellus, Ser. B 39, 439–458.

Rodi, W., 1980. Turbulence Models and Their Applications in Hydraulics. International Association Hydraulic Research, Delft, The Netherlands.

Rodi, W., 1987. Examples of calculation methods for flow and mixing in stratified fluids. J. Geophys. Res. 92, 5305–5328.

Sambrotto, R.N., Langdon, C., 1994. Water column dynamics of dissolved inorganic carbon (DIC), nitrogen and O_2 on Georges bank during April, 1990. Cont. Shelf Res. 14, 765–789.

Sambrotto, R.N., Savidge, G., Robinson, C., Boyd, P., Takahashi, T., Karl, D.M., Langdon, C., Chipman, D., Marra, J., Codispoti, L., 1993. Elevated consumption of carbon relative to nitrogen in the surface ocean. Nature 363, 248–250.

Stevens, B.B., Keeling, R.F., Heimann, M., Six, K.D., Murnane, R., Caldeira, K., 1998. Testing global ocean carbon cycle models using measurements of atmospheric O_2 and CO_2 concentration. Global Biogeochem. Cycles 12, 213–230.

Svensson, U., 1986. PROBE — an instruction manual, Report Oceanography. The Swedish Meteorological and Hydrological Institute (SMHI), S-601 76 Norrköping, Sweden, 90 pp.

Takahashi, T., Broecker, W.S., Langer, S., 1985a. Redfield ratio based on chemical data from isopycnal surfaces. J. Geophys. Res. 90, 6907–6924.

Takahashi, T., Olafsson, J., Broecker, W.S., Goddard, J., Chipman, D.W., White, J., 1985b. Seasonal variability of the carbon–nutrient chemistry in the oceanic areas west and north of Iceland. Rit Fiskildeildar, vol. 9, Marine Research Institute, Reykjavik, pp. 20–36.

Takahashi, T., Olafsson, J., Goddard, J.G., Chipman, D.W., Sutherland, S.C., 1993. Seasonal variation of CO_2 and nutrients in the high latitude surface oceans: a comparative study. Global Biogeochem. Cycles 7, 843–878.

Taylor, A.H., Watson, A.J., Robertson, J.E., 1992. The influence of the spring phytoplankton bloom on carbon dioxide and oxygen concentrations in the surface waters of the northeast Atlantic during 1989. Deep-Sea Res. 39, 137–152.

Visbeck, M., Marshall, J., Haine, T., Spall, M., 1997. Specification of eddy transfer coefficients in coarse-resolution ocean circulation models. J. Phys. Oceanogr. 27, 381–402.

Wanninkhof, R., 1992. Relationship between wind speed and gas exchange over the ocean. J. Geophys. Res. 97, 7373–7382.

Watson, A.J., Nightingale, P.D., Cooper, D.J., 1995. Modelling atmosphere–ocean CO_2 transfer. Philos. Trans. R. Soc. London, Ser. B 384, 125–132.

Weiss, R.F., 1974. Carbon dioxide in water and seawater: the solubility of a non-ideal gas. Mar. Chem. 2, 203–215.

Woolf, D.K., Thorpe, S.A., 1991. Bubbles and the air–sea exchange of gases in near-saturation conditions. J. Mar. Res. 49, 435–466.